analytical chemistry

pubs.acs.org/ac Article

Hydrogen Bond Organic Frameworks as a Novel Electrochemiluminescence Luminophore: Simple Synthesis and Ultrasensitive Biosensing

Nuo Zhang, Xin-Tao Wang, Zuping Xiong, Li-Yan Huang, Yu Jin, Ai-Jun Wang, Pei-Xin Yuan,* Ya-Bing He, and Jiu-Ju Feng*

Cite This: *Anal. Chem.* 2021, 93, 17110−17118 Read Online

ACCESS | Metrics & More | Article Recommendations | Supporting Information

Downloaded via TSINGHUA UNIV on November 5, 2022 at 20:46:19 (UTC).
See https://pubs.acs.org/sharingguidelines for options on how to legitimately share published articles.

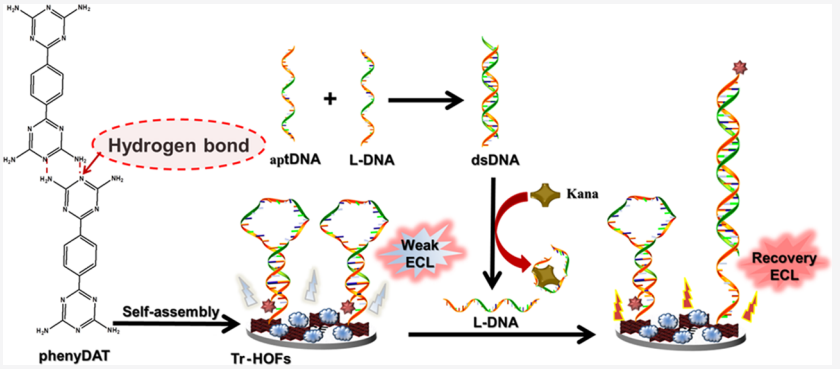

ABSTRACT: Nowadays, continuous efforts have been devoted to searching highly efficient electrochemiluminescence (ECL) emitters for applications in clinical diagnosis and food safety. In this work, triazinyl-based hydrogen bond organic frameworks (Tr-HOFs) were synthesized by N···H hydrogen bond self-assembly aggregation, where 6,6′-(1,4-phenylene)bis(1,3,5-triazine-2,4-diamine) (phenyDAT) was prepared *via* the cyclization reaction and behaved as a novel ligand. Impressively, the resulting Tr-HOFs showed strong ECL responses with highly enhanced ECL efficiency (21.3%) relative to the $Ru(bpy)_3^{2+}$ standard, while phenyDAT hardly showed any ECL emission in aqueous phase. The Tr-HOFs innovatively worked as a new ECL luminophore to construct a label-free biosensor for assay of kanamycin (Kana). Specifically, the ECL response greatly weakened upon assembly of captured DNA with ferrocene (cDNA-Fc) onto the Tr-HOFs-modified electrode, while the ECL signals were adversely recovered by releasing linked DNA (L-DNA) from double-stranded DNA (dsDNA, hybridization of aptamer DNA (aptDNA) with L-DNA) due to the specific recognition of Kana with the aptDNA combined by the linkage of L-DNA and cDNA-Fc on the electrode. The as-built sensor showed a broadened linear range (1 nM−10 μM) and a limit of detection (LOD) down to 0.28 nM, which also displayed satisfactory results in the analysis of Kana in the milk and diluted human serum samples. This work offers a novel pathway to design an ECL emitter with organic molecules, holding great promise in biomedical analysis and food detection.

INTRODUCTION

Electrochemiluminescence (ECL) does not need any external light sources, which can dramatically reduce the background noise, allowing control of the electrode potential and avoiding electrochemical interferences.[1,2] As an emerging and effective analytical method, ECL analysis attracts tremendous interest in clinical determinations of tumor biomarkers, bactericides, and antibiotics.[3,4] Briefly, ECL luminophores such as quantum dots,[5] organometallic complexes,[6] and tris(2,2′-bipyridyl)-ruthenium(II) ($Ru(bpy)_3^{2+}$)[7] play essential roles for transformation of electrical energy into radiative energy.

However, these conventional emitters either require complicated synthetic procedures or show the relatively lower ECL emission efficiency due to their $\pi-\pi$ stacking,[8] severely restricting their practical applications. Therefore, it is still significant yet challenging to develop facile methods for preparation of advanced ECL luminophores without molecule aggregation-caused quenching.

Nowadays, substantial attention has been drawn to metal−organic frameworks (MOFs) with conventional organic ECL emitters[9] as the ligand to chelate with the incorporated metal for boosting the ECL emission. With rigid hierarchical

Received: October 25, 2021
Accepted: December 8, 2021
Published: December 16, 2021

ACS Publications © 2021 American Chemical Society

https://doi.org/10.1021/acs.analchem.1c04608
Anal. Chem. 2021, 93, 17110−17118

Scheme 1. (A) Preparation Scheme of Tr-HOFs with PhenyDAT as a Ligand and (B) Diagram for Construction of the Label-Free ECL Biosensor for Kana Detection

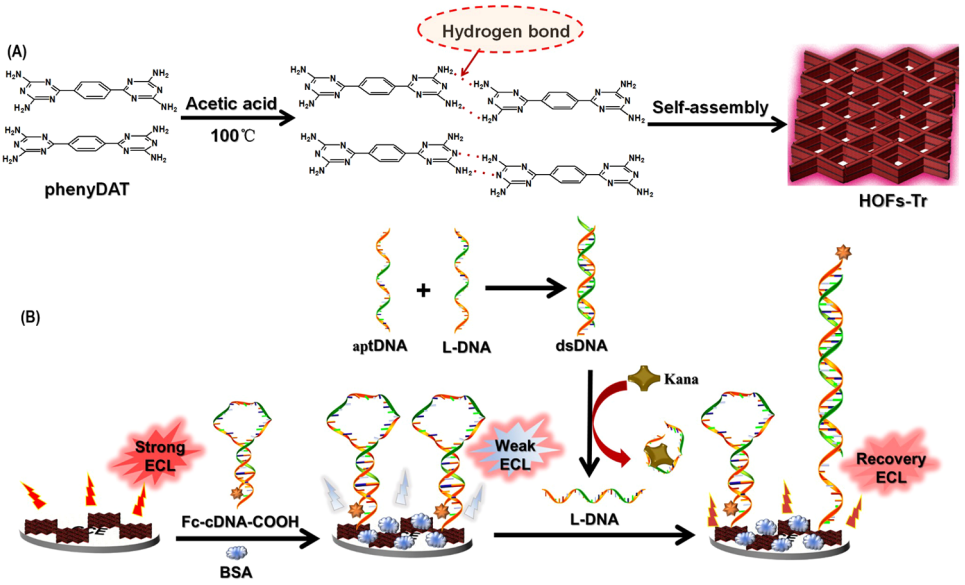

frameworks,[10] the exchange between the charge and energy of the ligand units is enhanced accordingly. In addition, Au nanoclusters (Au NCs)[11] and Pd nanocones[12] are all identified as ECL luminescent nanomaterials to gain anode and cathode radiation. For most of the nanomaterials, the unique ECL signals are mainly originated from the excellent electron transfer and abundant surface active sites for catalysis of $K_2S_2O_8$ or tripropylamine (TPA) as coreactants.[13]

Lately, the aggregation-induced ECL (AIECL) characteristics provide a pioneering pattern to acquire novel ECL materials.[14] Notably, heterocyclic compounds[15] and supramolecules[16] have been exploited as ECL emitters in aqueous systems, greatly abolishing the detrimental quenching stacking. Unfortunately, the high cost and tedious synthesis of AIECL molecules and organic ligands[17] still hamper the advancement of ECL applications in bioassays. In the AIE mechanism, such organic molecules show weak fluorescence (FL) in an aqueous states but emit strong FL signals in the aggregated cases.[18] Inspired by this, a series of ECL organic emitters were developed by regulating the aggregation states and network-like assembly.[19]

By contrast, many commonly N-rich heterocyclic complexes such as 2,4-diaminotriazinyl (DAT)[20] hold great promise for electrochemical and luminescence applications, owing to their intrinsic advantages of low cost and easy preparation as well as more lone-pair electrons.[21] Meanwhile, the N-rich groups offer extensive units for self-assembly of such aggregation and block the nonradioactive decay of luminogens.[22]

As a new family of porous network-like materials, hydrogen bond organic frameworks (HOFs) are gradually self-assembled from organic ligands *via* hydrogen-bonding interactions,[23] which display particular applications in gas storage, chiral separation, and molecular recognition.[24] Unlike other types of organic frameworks, the assembled HOFs can be facilely prepared by recrystallization, which exhibit huge structure flexibility.[25] The triazinyl HOFs (Tr-HOFs) emerge by self-assembly of the N···H bonded aggregation with dual DAT derivatives as the ligands.[26] The shorter bond length and the highly specific molecular orientation endow the decay in the $\pi-\pi$ stacking of the ligand, which contributes to the variation in the photoelectric habits.[27] Additionally, the unique network-like architectures of the HOFs provide sufficient surface active sites for the site-to-site transport of energy and electrons, thereby harvesting the enhanced ECL emission.

As we know, kanamycin (Kana) is an antibiotic, which is one of the most important antibacterial agents and has serious rampant usage in drugs and food.[28,29] In this work, Tr-HOFs were prepared by self-assembly through slow crystallization, using 6,6′-(1,4-phenylene)bis(1,3,5-triazine-2,4-diamine) (phenyDAT, initially synthesized by the cyclization reaction) as the ligand (Scheme 1A). Employing the Tr-HOFs as the ECL emitter, a label-free ECL biosensor was then built, combined by linking captured DNA initially grafted with ferrocene (cDNA-Fc) as the quencher. The quantitative determination of Kana was achieved by the definitely recovered ECL signals *via* release of the linked DNA (L-DNA) from double-stranded DNA (dsDNA, hybridization between aptamer DNA (aptDNA) and L-DNA) and the specific recognition of Kana with its aptDNA (Scheme 1B). Such bioanalysis of Kana was realized even in the milk and diluted human serum samples.

EXPERIMENTAL SECTION

Synthesis of PhenyDAT. PhenyDAT behaved as a ligand, which was prepared according to the previous study.[30] In brief, 0.772 g of 1,4-dicyanobenzene (DAB, 4.6 mmol) was dissolved into 20 mL of dimethylformamide (DMF), followed by putting 2.024 g of dicyandiamide (24 mmol) and 0.562 g of KOH (10 mmol) into 80 mL of DMF. Then, the two solutions were mixed homogeneously in a 250 mL round-bottom flask and refluxed at 140 °C for 15 h under continuous stirring in a N_2 atmosphere. After completely washing with methanol, the product of phenyDAT powder was obtained *via* vacuum drying, with a yield of about 81%. The molecular formula was $C_{12}H_{12}N_{10}$. ^{1}H NMR (600 MHz, DMSO): δ (ppm) 8.32 (s, 4H), 6.82 (s, 8H). ^{13}C NMR (150 MHz, DMSO): δ (ppm) 170.22, 167.86, 139.90, 127.93.

https://doi.org/10.1021/acs.analchem.1c04608
Anal. Chem. 2021, 93, 17110−17118

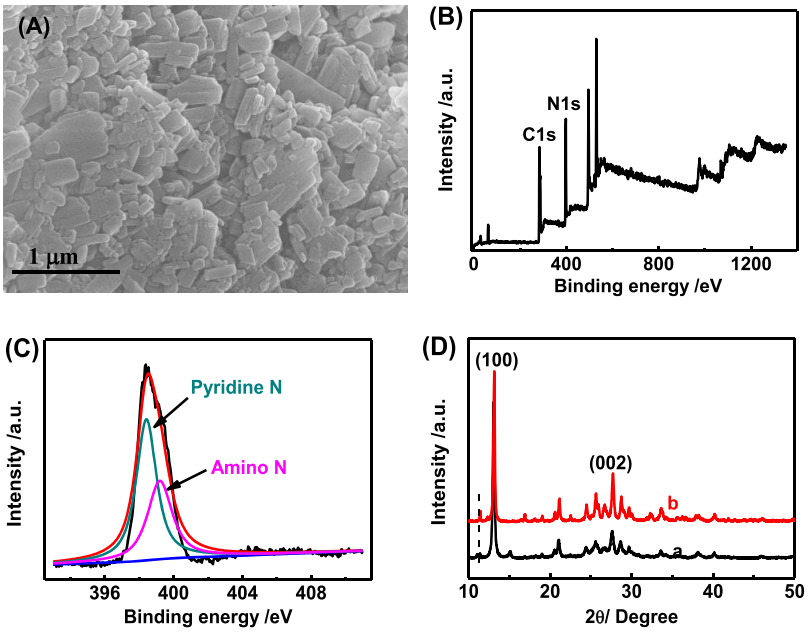

Figure 1. (A) SEM image and (B) survey XPS spectrum of Tr-HOFs. (C) High-resolution N 1s XPS segment of Tr-HOFs. (D) XRD spectra of Tr-HOFs (curve a) and phenyDAT (curve b).

Construction of Tr-HOFs. The Tr-HOFs were harvested from the hydrogen bond self-assembly aggregation, which was illustrated as follows:[27] phenyDAT was dissolved into acetic acid, heated up to 100 °C, and retained for 5 h. Then, the solution was cooled down slowly to gain the precipitate and thoroughly washed with water. After drying in vacuum, the Tr-HOFs powder was harvested with the crystal data described as below (M = N/A g/mol): monoclinic, space group Cc (no. 9), a = 16.4748 Å, b = 23.4369 Å, c = 11.9144 Å, α = 90.000°, β = 102.891°, γ = 90.000°, V = 4484.4207 Å^3, Z = 1, N/A reflection measured (N/A° ≤ 2Θ ≤ N/A°), and N/A unique (R_{int} = N/A, R_{sigma} = N/A), which were used in all calculations. The final R_1 was N/A (N/A), and wR_2 was N/A (all data).

Construction of the Label-Free ECL Biosensor. Prior to use, a glassy carbon electrode (GCE, 5 mm in diameter) was polished with 0.05 μm alumina solution and then washed with water to obtain a mirror-like surface. Then, 20 μL of the Tr-HOFs suspension (0.5 μg mL^{-1}) was uniformly deposited onto the electrode. To activate the carboxyl, 0.4 M 1-(3-dimethylaminopropyl)-3-ethylcarbodiimide (EDC) and 0.1 M *N*-hydroxyl succinimide (NHS) were dropped into 1 μM cDNA solution, combined by casting them onto the Tr-HOFs-modified electrode at 4 °C for 12 h to form the amide bonds. Subsequently, 20 μL of bovine serum protein (BSA) solution (1.0 wt %) was cast onto the electrode and incubated for 2 h at 37 °C to block nonspecific binding sites. Finally, 0.5 mL of the 1 μM L-DNA and aptDNA solutions was heated at 95 °C for 5 min and then cooled down to room temperature. The above solutions were mixed with different concentrations of Kana to achieve the biorecognition after incubation for 45 min at 37 °C in each case, accompanied by operating the ECL detection experiments.

Notably, the modified electrode was thoroughly rinsed with sterilized phosphate buffer solution (PBS, pH 7.4, 10 mM) after each step throughout the inspection process to remove the excess unbound material. Unless declared otherwise, the ECL signals were recorded in the PBS with a scan rate of 100 mV s^{-1} in the range of 0.0−1.4 V with a photomultiplier tube (PMT) voltage of 800 V.

RESULTS AND DISCUSSION

Morphological and Structural Characterizations of Tr-HOFs. To carefully examine the morphological and structural features of Tr-HOFs, scanning electron microscopy (SEM) measurements were first performed. As revealed by the SEM image (Figure 1A), plenty of well-distributed cuboid-like structures show up with a vertical orientation and a smooth surface. Interestingly, there hardly emerges any lattice fringe, which confirms its amorphous characteristic upon orderly self-assembly accumulation.[31] By comparison, pure phenyDAT without slow crystallization does not show any network-like structure (Figure S1A).

X-ray photoelectron spectroscopy (XPS) measurements were conducted to attain more structural information on advanced nanomaterials.[32] In the survey XPS spectrum of Tr-HOFs, there are obvious peaks located at 284.86 and 402.56 eV, which are attributed to the C and N elements, respectively, in good accordance with the elemental compositions of Tr-HOFs (Figure 1B).[33] Meanwhile, the two peaks show up at 398.42 and 399.28 eV in the high-resolution N 1s XPS section (Figure 1C), belonging to the triazinyl N and amino N, respectively. Importantly, the peak intensity of the triazinyl N is larger than that of the amino N, illustrating the essential role of the triazinyl played in the Tr-HOFs.[34]

X-ray diffraction (XRD) analysis was conducted to critically characterize the crystal structures of Tr-HOFs and phenyDAT.[35] There are two representative diffraction peaks emerged at 13.1 and 27.41° for both Tr-HOFs and phenyDAT (Figure 1D), which are well-indexed to the (100) and (002) planes corresponding to the characteristic interlayer structural and interplanar staking of aromatic systems,[36] respectively. However, the peaks of Tr-HOFs are less than those of phenyDAT, indicating the unique structured aggregation of the ligands in HOFs.

https://doi.org/10.1021/acs.analchem.1c04608
Anal. Chem. 2021, 93, 17110−17118

Importantly, the peak of the Tr-HOFs at 11.24° (attributed to the C-based nanomaterial) shows a half-fold relative peak intensity (0.042/0.078) by contrast with that of phenyDAT, which indicates the less C-based accumulated planes formed in slow crystallization. It demonstrates that such orderly aggregation effectively avoids the detrimental stacking.

The Molecule and Crystal Structure of Tr-HOFs. Scheme 2 illustrates the schematic route for synthesis of the phenyDAT ligand, whose structure was first confirmed by ^{1}H NMR and ^{13}C NMR spectroscopy. The phenyl and triazine protons appear at 8.32 and 6.82 ppm (Figure S2A), respectively. Also, the classical carbon atoms of the triazine ring and the aromatic pyrene moiety all emerge at 167.86 and 127.93 ppm (Figure S2B),[37] respectively, in good agreement with the standard structure of phenyDAT.

Scheme 2. Synthesis of PhenyDAT

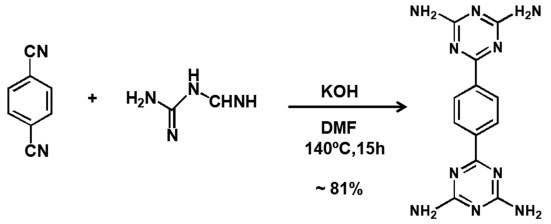

As unveiled by the single-crystal X-ray diffraction analysis (Figure 2A,B), the Tr-HOFs belong to the monoclinic system with the *Cc* space group, where the Hirshfeld surfaces of HOFs were mapped over normal distribution (d_{norm}).[38] Specifically, the larger red spots indicate the strong intermolecular interactions between the molecules, while the smaller ones correlate to their weak interactions. Moreover, the planar ligand of phenyDAT shows the symmetrical DAT motifs with cavity N and amino, coupled by intermolecular integration of the six surrounding phenyDAT with the core motifs.

The Hirshfeld surfaces of these phenyDAT derivatives are almost blue, while many N sites are red,[39] suggesting the stronger N···H bond at most of the intermolecular contacts with a bond length of about 2.57 Å. These contacts comprise 31.7% of the N···H bond on the total Hirshfeld surfaces for phenyDAT, without any C−C bond observed (Figure S1B), which accounts for the main formation of the hydrogen bond by self-assembly, rather than the $\pi-\pi$ stacking of the ligands.[40] These synthon units are self-assembled together, in turn forming the supramolecular 3D porous network, reflecting huge potential for interfacial electron and energy transfer between the HOFs and buffer (Figure 2C).

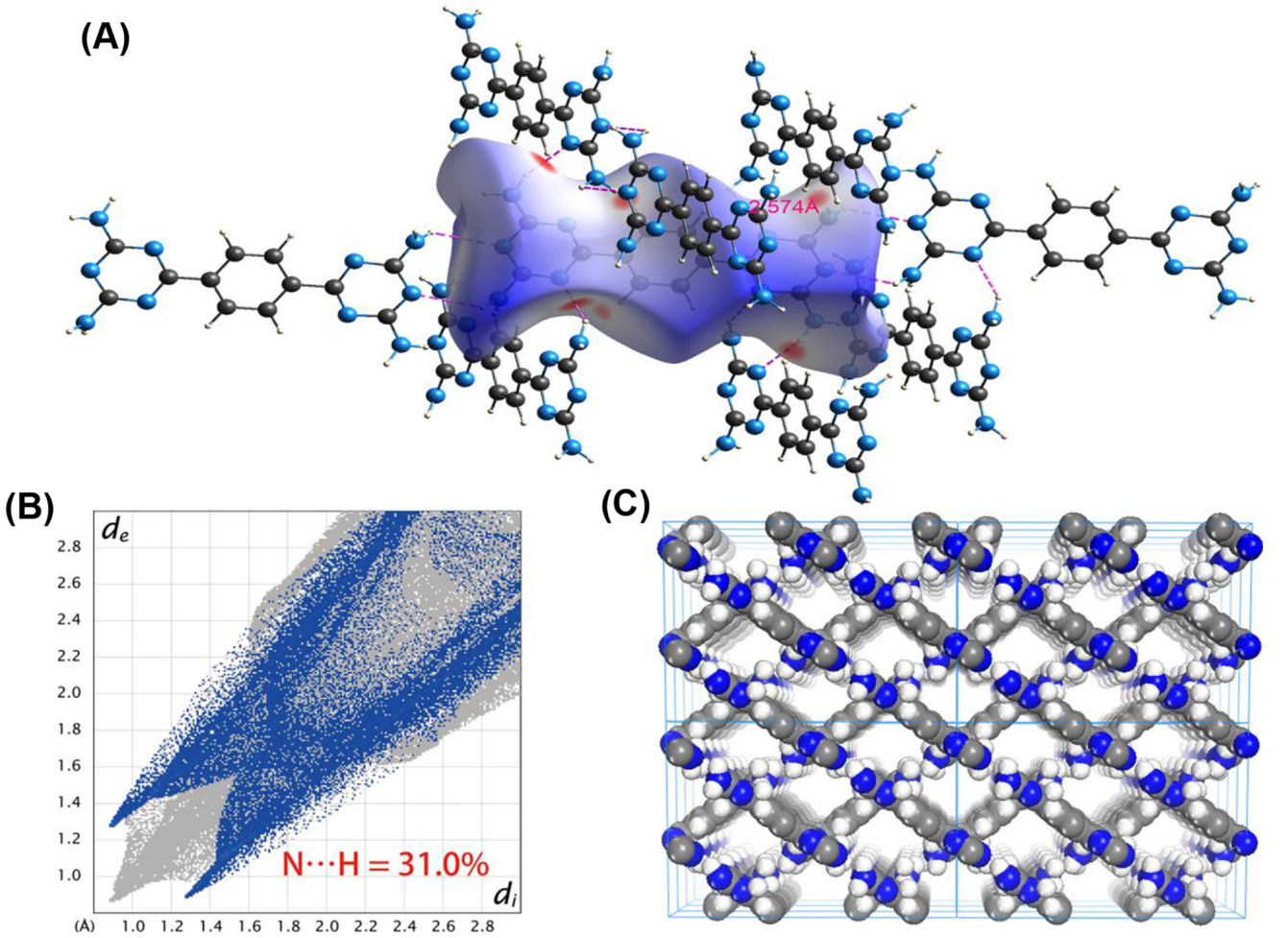

Figure 2. (A) Intermolecular interactions of phenyDAT in Tr-HOFs with the labeled distance extracted from its crystal packing data. (B) View of the Hirshfeld surface mapped over d_{norm} of the N−H bond for phenyDAT in Tr-HOFs. (C) 3D packing framework of Tr-HOFs.

https://doi.org/10.1021/acs.analchem.1c04608
Anal. Chem. 2021, 93, 17110−17118

Optical Characterization of Tr-HOFs. To explore the optical properties of Tr-HOFs, the UV−vis spectrum was first provided (Figure 3A). In brief, there is a classical absorbance inflection point located at 376 nm for the conjugated aggregation structure (curve a).[41] Nevertheless, the inflection point is centered at 353 nm for the phenyDAT molecule (curve b), indicating its unstable energy level state in dimethyl sulfoxide (DMSO) solution. Additionally, DAB hardly shows any absorbance within the same wavelength region (curve c).

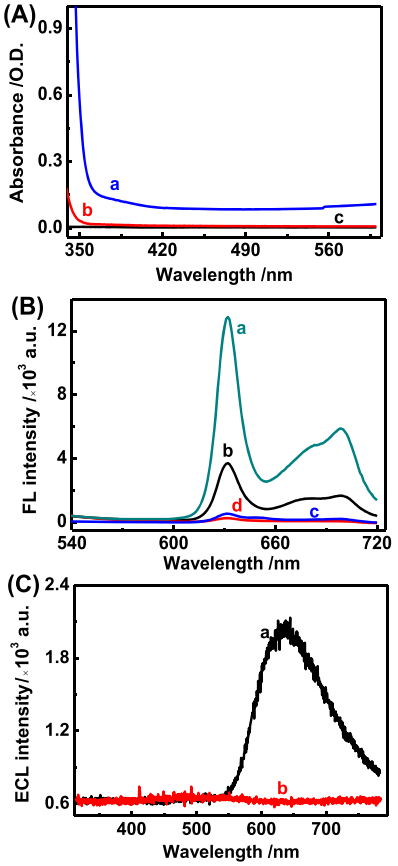

Figure 3. (A) UV−vis spectra of Tr-HOFs (curve a), phenyDAT (curve b), and DAB (curve c). (B) FL spectra of Tr-HOFs with TPA (curve a), Tr-HOFs (curve b), DAB (curve c), and dicyandiamide (curve d). (C) ECL spectra of Tr-HOFs (curve a) and phenyDAT (curve b) in the detection system containing 13 mM TPA.

In addition, obvious FL emission shoulder peaks emerge at 633 (1.95 eV, peak I) and 698 nm (1.77 eV, peak II) for Tr-HOFs under an excitation wavelength of 390 nm (Figure 3B, curve a), while two feeble FL emission peaks appear at 633 and 698 nm either for phenyDAT (Figure 3B, curve b) or DAB (Figure 3B, curve c) under the same conditions. Interestingly, the FL intensity of the shoulder peak increases violently for the Tr-HOFs at 13 mM TPA (Figure 3B, curve d), explaining the large increase in the involved electron amount of the as-built Tr-HOFs with TPA.[12]

The ECL spectrum of Tr-HOFs shows an evident emission peak at 643 nm (1.92 eV, Figure 3C, curve a) in the detection solution containing TPA, which exhibits the redshift (about 10 nm) relative to that of the FL peak I, owing to their various excitation pathways. Also, a very weak luminescence is noticed for phenyDAT in the same surroundings (Figure 3C, curve b), illustrating the importance of the N···H bond self-assembly aggregation of the Tr-HOFs as the ECL emitter.

The ECL Mechanism of the Tr-HOFs in the TPA System. The ECL experiments and the corresponding CV tests were carefully conducted to investigate the ECL mechanism of the Tr-HOFs/TPA system.[42] There is a weak anodic ECL peak detected at 1.38 V with an intensity of 20 a.u. for pure Tr-HOFs (PMT is 1000 V, Figure 4A, curve a), which confirms the as-prepared HOFs as an efficient ECL emitter. Meanwhile, the corresponding CV plots show a pair of quasi-reversible redox peak at 0.72/0.58 V, thanks to the redox reaction of triazinyl HOFs (Figure 4B, curve a).

However, phenyDAT scarcely displays any ECL response (Figure 4A, curve b) and redox peaks (Figure 4B, curve b), thanks to the disorderly accumulation and nonradiative decay. Also, it hardly detects any ECL response with the present DAB (Figure S3A, curve a) or dicyandiamide (Figure S3A, curve b).

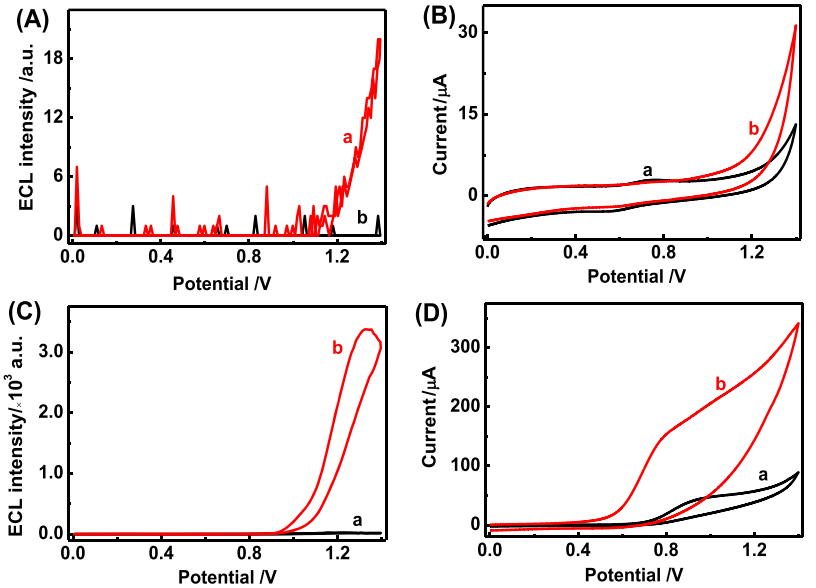

Figure 4. ECL (A,C) and CV (B,D) plots of Tr-HOFs (curve a) and phenyDAT (curve b) without (A,B) and with (C,D) TPA in the detection system.

https://doi.org/10.1021/acs.analchem.1c04608
Anal. Chem. 2021, 93, 17110−17118

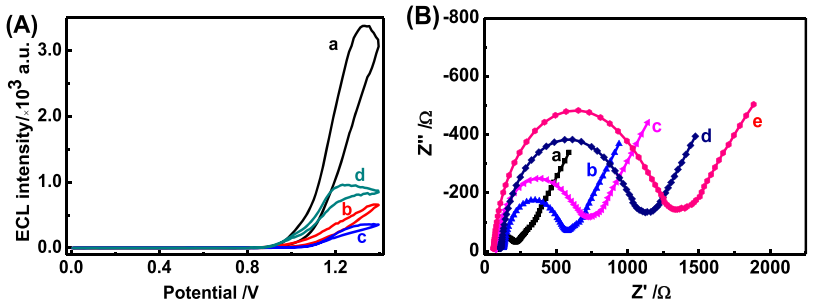

Figure 5. (A) ECL signals of Tr-HOFs/GCE (curve a), cDNA/(a) (curve b), BSA/(b) (curve c), and Kana+dsDNA/(c) (curve d). (B) Nyquist plots of bare GCE (curve a), Tr-HOFs/(a) (curve b), cDNA/(b) (curve c), BSA/(c) (curve d), and Kana+dsDNA/(d) (curve e) in 0.1 M KCl solution containing 5 mM $[Fe(CN)_6]^{3-/4-}$.

These observations demonstrate that the unique frame-like structures of Tr-HOFs play the key role for the excitation of the surface electrons.

Moreover, the cathode emission peak emerges at 1.28 V for the ECL measurement of the Tr-HOFs in a dichloromethane (DCM) electrolyte containing 0.2 M tetrabutylammonium perchlorate (TBAP, Figure S3B). The corresponding CV plots exhibit two reversible redox peaks at −0.68/−0.78 V and 1.18/1.02 V (Figure S3C), attributed to the formation of [Tr-HOFs]$^{\bullet-}$ and the cation [Tr-HOFs]$^{+}$,[43,44] respectively.

Importantly, the enthalpy energy ($-\Delta H$ in eV) is calculated to be 1.86 eV (see details in the Apparatus section, eq S1, SI), which is nearly equal to the energy of the FL peak I and ECL emission. Meanwhile, the blank TPA sample fails to detect any ECL emission (Figure 4C, curve a), but a classical oxidation peak appears at 0.93 V corresponding to the oxidation of TPA to TPA^{+} (Figure 4D, curve a). Finally, the ECL peak of Tr-HOFs is located at 1.23 V with a strong intensity of 3395 a.u. (Figure 4C, curve b), coupled with the oxidation peak at 0.84 V on the CV curve (Figure 4D, curve b) in the Tr-HOFs/TPA system, revealing TPA as the prominent coreactant.

After accurate integral calculation (see details in the Apparatus section, eq S2, SI), the ECL efficiency of the Tr-HOFs/TPA is about 0.413, by using $Ru(bpy)_3^{2+}/C_2O_4^{2-}$ as a standard (0.0185),[45] which is about 21.3% of the standard $Ru(bpy)_3^{2+}$/TPA system (1.940), displaying the excellent luminescence property of the Tr-HOFs.[46] Hence, the ECL emission of the Tr-HOFs/TPA system follows the "oxidation−reduction" route, as depicted by the following equations:

$$\text{Tr} - \text{HOFs} - e^- \rightarrow \text{Tr} - \text{HOFs}^+ (\text{at } 0.72 \text{ V}) \quad (1)$$

$$\text{TPA} - e^- \rightarrow \text{TPA}^{\bullet+} (\text{at } 0.93 \text{ V}) \quad (2)$$

$$\text{TPA}^{\bullet+} - H^+ \rightarrow \text{TPA}^{\bullet} \quad (3)$$

$$\text{Tr} - \text{HOFs}^+ + \text{TPA}^{\bullet} \rightarrow \text{Tr} - \text{HOFs}^* + P_1 \quad (4)$$

$$\text{Tr} - \text{HOFs}^* \rightarrow \text{Tr} - \text{HOFs} + h\nu (\lambda = 643 \text{ nm}) \quad (5)$$

Feasibility of the Label-Free Biosensor. According to the ECL procedures of the as-synthesized emitter, the feasibility of this sensor was first studied by electrochemical impedance spectroscopy (EIS), where the semicircle diameter on the Nyquist plot refers to the electron transfer resistance (R_{et}) associated with the difficulty of interfacial electron transport between the electrode and the solution by employing ferricyanide redox as a probe.[47] As shown in Figure 5A, the R_{et} value increases obviously upon modification of the Tr-HOFs (curve b) over the freshly cleaned GCE (curve a). Then, the R_{et} is enhanced continuously by the sequential assembly of cDNA-Fc (curve c) and BSA (curve d) for their insulated electrical conductivity. After further contact with the ds-DNA (formed by L-DNA with aptDNA) and Kana in the aqueous solution, the R_{et} enlarges distinctly (curve e), on account of the severely restricted electron transfer by such biomaterials.

Also, Figure 5B displays the ECL responses toward the stepwise construction of the sensor in the detection environment. The largest ECL signal is observed after immobilization of the Tr-HOFs, owing to their excellent ECL property (curve a). After assembly of the cDNA-Fc *via* amide bonds, the ECL intensity is quenched definitely (curve b) due to the strong interactions of cDNA-Fc with this luminophore. Then, the ECL signals continuously decrease by the follow-up combination with BSA (curve c), thanks to its poor conductivity.[48] Lastly, the ECL signal is adversely recovered (28.5%, curve d) by contacting with the dsDNA and Kana in the detection system. Briefly, the L-DNA is released from the dsDNA, which further hybridizes with the cDNA-Fc to generate the rigid structures again on the electrode *via* specific recognition of the aptDNA with Kana. Hence, these scenarios confirm the successful fabrication and excellent feasibility of the ECL sensing setups.

Optimization of the ECL Detection System. To evaluate the analytical performance of the as-fabricated ECL sensor, the deposited Tr-HOFs amount closely correlates to the ECL responses (Figure S4A).[31] Specifically, the ECL signals increase regularly with the enlarged amount of Tr-HOFs, reach the maximum at a Tr-HOFs concentration of 0.5 μg mL^{-1}, and display a downtrend in the ECL responses at the higher Tr-HOFs concentration due to the seriously restricted electron transfer between this emitter and the electrode.[49]

The TPA concentration is also an important parameter toward the ECL performances of emitters.[50] Hence, Figure S4B exhibits the ECL intensity of the Tr-HOFs-modified electrode toward various TPA concentrations. The ECL responses are enhanced obviously from 8 to 13 mM and achieve the apex point at 13 mM. After that, the ECL signals remain steady, thanks to the saturated combination of the luminophore and TPA.[51]

Lastly, the incubation time plays a critical role for the integration of the target with the aptamer.[52] As displayed in Figure S4C, the ECL intensities show a dramatic increase by extending the time, accompanied by a slight attenuation at 45 min due to the saturated recognition of Kana with the aptamer. As a result, 0.5 μg mL^{-1} Tr-HOFs, 13 mM TPA, and an incubation time of 45 min were adopted for the sequential Kana detection.

https://doi.org/10.1021/acs.analchem.1c04608
Anal. Chem. 2021, 93, 17110−17118

Assay of Kana on the ECL Biosensor. Under the optimal detection conditions, the ECL curves were acquired on the sensor at different Kana concentrations. As seen in Figure 6A,

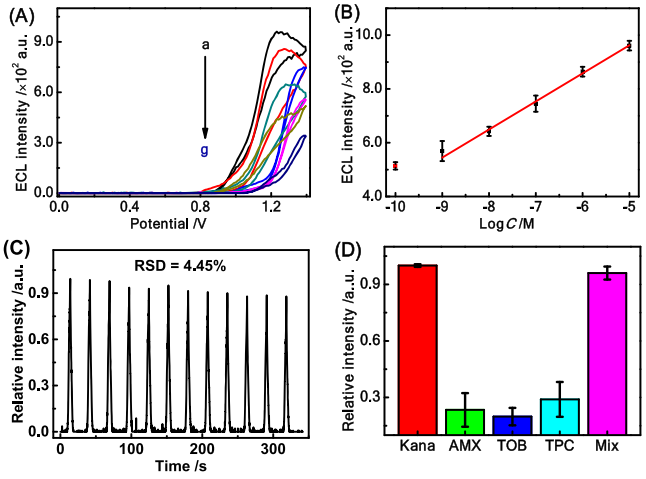

Figure 6. (A) ECL signals acquired at Kana concentrations ranging from 10 μM to 0.1 nM (curves a–g). (B) Calibration curve. (C) Consecutive scans of the as-developed ECL biosensor. (D) Relative ECL responses of the biosensor toward different interferences and targets.

the ECL responses increase gradually by elevating the Kana concentrations in the range of 0.1 nM–10 μM. Also, the ECL signals are proportional to the Kana concentrations from 1 nM to 10 μM, reflecting their excellent linear relationship.

The linear fitting equation is described as $I = 100.6 \log c + 1460.4$ with a good correlation coefficient (R^2) of 0.994 (Figure 6B), in which each concentration point is detected for at least 3 times to guarantee the reproducibility.[53] Herein, I stands for the ECL response, and c is the concentration of Kana. Also, the detection of limit (LOD) is as low as 0.28 nM according to the 3 times signal-to-noise (3 S/N) ratio of the blank response.[54] In contrast with most of the previous biosensors (see details in Table S1), the as-established sensor exhibits a broadened linear range and a lower LOD, chiefly resulted from the bright ECL emission of the Tr-HOFs and the efficient sensing setups *via* the highly specific recognition of Kana with the aptDNA.

Beyond the above, the ECL intensity was marked under the continuous 10 cycle scan to further evaluate the operation stability. As illustrated in Figure 6C, the relative ECL intensity remains constant during the operating period. Notably, the relative standard deviation (RSD) is around 4.44%, which demonstrates the remarkable stability in this determination.

Some potential antibiotics such as thiamphenicol (TAP), amoxicillin (AMC), tobramycin (TOB), and their mixture with Kana (Mix+Kana) were chosen to validate the selectivity (Figure 6D). Notably, the relative ECL intensity of each single interference lowers to 20% of Kana itself, which is equal to that of the Mix+Kana sample, showing the accepted selectivity.[55] As a result, the constructed sensor reveals exceptional reliability and specificity due to the highly specific recognition of the aptamer with the target that is essential for developing advanced ECL setups toward Kana detection.

Analysis of Real Samples. The practicability and applicability of the as-built sensor were further evaluated in the milk and 100-fold diluted serum samples. Observably, there was hardly any detected ECL response for the practical samples in the above detection conditions, so a standard addition method[48] was employed in the Kana concentration scope of 1 nM–1 μM. In brief, the biosensor shows a satisfactory recovery mainly centered between 92.00 and 108.30% for the milk sample, with the RSD less than 6.40% (Table S2). In addition, the recoveries emerge in the range of 97.70–108.42% toward the 100-fold diluted serum sample with the RSD below 3.59% (Table S3). Taking these into account, the sensor holds substantial promise in food assay and clinical diagnosis.

CONCLUSIONS

In this work, the Tr-HOFs were prepared *via* intermolecular N···H bond self-assembly aggregation, with phenyDAT (synthesized by the cyclization reaction) as the ligand. For the eliminated π–π stacking of ligands, the as-formed Tr-HOFs exhibited the superior anode ECL emission with an ECL efficiency of 21.3% relative to the $Ru(bpy)_3^{2+}$, unlike phenyDAT without any ECL response. For that, a label-free ECL biosensor was constructed by sequential assembly of cDNA-Fc *via* amide reaction, inducing the severe decay in the ECL signals. Afterward, the ECL response was inversely recovered by releasing L-DNA from the dsDNA, coupled by the efficient linkage of the L-DNA and cDNA-Fc on the electrode. The as-built aptasensor displayed a widened linear range of 1 nM–10 μM (R^2 = 0.994) with an LOD of 0.28 nM, acceptable selectivity, and stability as well as practical applications in milk and diluted human serum samples. Hence, this work provides an effective method for harvesting a powerful ECL luminophore with organic molecules, which would greatly expand the optical applications of HOFs in the future.

ASSOCIATED CONTENT

Supporting Information

The Supporting Information is available free of charge at https://pubs.acs.org/doi/10.1021/acs.analchem.1c04608.

Experimental section and apparatus; SEM images, Hirshfeld surface, ^{1}H NMR and ^{13}C NMR spectra, and ECL experiments of DAB and dicyandiamide; detection condition optimization; comparison of the as-fabricated aptasensor for determination of Kana with others reported earlier and detection results of Kana in milk and 100-fold diluted serum samples (PDF)

Crystallographic information on Tr-HOFs (CIF)

AUTHOR INFORMATION

Corresponding Authors

Pei-Xin Yuan – *Key Laboratory of the Ministry of Education for Advanced Catalysis Materials, College of Chemistry and Life Sciences, College of Geography and Environmental Sciences, Zhejiang Normal University, Jinhua 321004, China;* orcid.org/0000-0002-4585-323X; Email: ypxdr@zjnu.edu.cn

Jiu-Ju Feng – *Key Laboratory of the Ministry of Education for Advanced Catalysis Materials, College of Chemistry and Life Sciences, College of Geography and Environmental Sciences, Zhejiang Normal University, Jinhua 321004, China;* orcid.org/0000-0002-7954-0573; Email: jjfeng@zjnu.cn

https://doi.org/10.1021/acs.analchem.1c04608
Anal. Chem. 2021, 93, 17110–17118

Authors

Nuo Zhang − *Key Laboratory of the Ministry of Education for Advanced Catalysis Materials, College of Chemistry and Life Sciences, College of Geography and Environmental Sciences, Zhejiang Normal University, Jinhua 321004, China*

Xin-Tao Wang − *Key Laboratory of the Ministry of Education for Advanced Catalysis Materials, College of Chemistry and Life Sciences, College of Geography and Environmental Sciences, Zhejiang Normal University, Jinhua 321004, China*

Zuping Xiong − *Key Laboratory of the Ministry of Education for Advanced Catalysis Materials, College of Chemistry and Life Sciences, College of Geography and Environmental Sciences, Zhejiang Normal University, Jinhua 321004, China*; orcid.org/0000-0003-2661-6615

Li-Yan Huang − *Key Laboratory of the Ministry of Education for Advanced Catalysis Materials, College of Chemistry and Life Sciences, College of Geography and Environmental Sciences, Zhejiang Normal University, Jinhua 321004, China*

Yu Jin − *Key Laboratory of the Ministry of Education for Advanced Catalysis Materials, College of Chemistry and Life Sciences, College of Geography and Environmental Sciences, Zhejiang Normal University, Jinhua 321004, China*

Ai-Jun Wang − *Key Laboratory of the Ministry of Education for Advanced Catalysis Materials, College of Chemistry and Life Sciences, College of Geography and Environmental Sciences, Zhejiang Normal University, Jinhua 321004, China*; orcid.org/0000-0003-2041-7981

Ya-Bing He − *Key Laboratory of the Ministry of Education for Advanced Catalysis Materials, College of Chemistry and Life Sciences, College of Geography and Environmental Sciences, Zhejiang Normal University, Jinhua 321004, China*

Complete contact information is available at: https://pubs.acs.org/10.1021/acs.analchem.1c04608

Notes

The authors declare no competing financial interest.

■ ACKNOWLEDGMENTS

This research was supported by the Natural Science Foundation of Zhejiang Province (no. LQ19B050004), the Basic Public Welfare Research Project of Zhejiang Province (no. LGG19B050001), and the Open Research Fund of the Key Laboratory of the Ministry of Education for Advanced Catalysis Materials (Zhejiang Normal University).

■ REFERENCES

(1) Maar, R. R.; Zhang, R.; Stephens, D. G.; Ding, Z.; Gilroy, J. B. *Angew. Chem., Int. Ed.* **2019**, *58*, 1052−1056.

(2) Hou, K.; Puzzo, D.; Helander, M. G.; Lo, S. S.; Bonifacio, L. D.; Wang, W.; Lu, Z.-H.; Scholes, G. D.; Ozin, G. A. *Adv. Mater.* **2009**, *21*, 2492−2496.

(3) Wu, M.-S.; Yuan, D.-J.; Xu, J.-J.; Chen, H.-Y. *Chem. Sci.* **2013**, *4*, 1182−1188.

(4) Nie, Y.; Yuan, X.; Zhang, P.; Chai, Y.; Yuan, R. *Anal. Chem.* **2019**, *91*, 3452−3458.

(5) Yan, Y.; Gong, J.; Chen, J.; Zeng, Z.; Huang, W.; Pu, K.; Liu, J.; Chen, P. *Adv. Mater.* **2019**, *31*, 1808283.

(6) Ma, C.; Wu, S.; Zhou, Y.; Wei, H.-F.; Zhang, J.; Chen, Z.; Zhu, J.-J.; Lin, Y.; Zhu, W. *Angew. Chem., Int. Ed.* **2021**, *60*, 4907−4914.

(7) Wang, Y.; Guo, W.; Yang, Q.; Su, B. *J. Am. Chem. Soc.* **2020**, *142*, 1222−1226.

(8) Gu, J.; Gao, Y.; Wu, J.; Li, Q.; Li, A.; Zhang, W.; Dong, H.; Wen, B.; Gao, F.; Zhao, Y. S. *ACS Appl. Mater. Interfaces* **2017**, *9*, 8891−8899.

(9) Jin, Z.; Zhu, X.; Wang, N.; Li, Y.; Ju, H.; Lei, J. *Angew. Chem., Int. Ed.* **2020**, *59*, 10446−10450.

(10) Sun, L.; Chen, Y.; Duan, Y.; Ma, F. *ACS Appl. Mater. Interfaces* **2021**, *13*, 38923−38930.

(11) Yu, L.; Zhang, Q.; Kang, Q.; Zhang, B.; Shen, D.; Zou, G. *Anal. Chem.* **2020**, *92*, 7581−7587.

(12) Wang, H.-M.; Wang, C.-C.; Wang, A.-J.; Zhang, L.; Luo, X.; Yuan, P.-X.; Feng, J.-J. *Sens. Actuator B Chems.* **2019**, *281*, 588−594.

(13) Zhai, Q.; Li, J.; Wang, E. *ChemElectroChem* **2017**, *4*, 1639−1650.

(14) Carrara, S.; Aliprandi, A.; Hogan, C. F.; De Cola, L. *J. Am. Chem. Soc.* **2017**, *139*, 14605−14610.

(15) Gao, H.; Zhang, N.; Pan, J.-B.; Quan, Y.-X.; Cheng, Y.; Chen, H.-Y.; Xu, J.-J. *ACS Appl. Mater. Interfaces* **2020**, *12*, 54012−54019.

(16) Zhang, Y.; Zhao, Y.; Han, Z.; Zhang, R.; Du, P.; Wu, Y.; Lu, X. *Angew. Chem., Int. Ed.* **2020**, *59*, 23261−23267.

(17) Guo, J.; Feng, W.; Du, P.; Zhang, R.; Liu, J.; Liu, Y.; Wang, Z.; Lu, X. *Anal. Chem.* **2020**, *92*, 14838−14845.

(18) Wang, H.; Li, Q.; Zhang, J.; Zhang, H.; Shu, Y.; Zhao, Z.; Jiang, W.; Du, L.; Phillips, D. L.; Lam, J. W. Y.; Sung, H. H. Y.; Williams, I. D.; Lu, R.; Tang, B. Z. *J. Am. Chem. Soc.* **2021**, *143*, 9468−9477.

(19) Zhang, J.-L.; Yang, Y.; Liang, W.-B.; Yao, L.-Y.; Yuan, R.; Xiao, D.-R. *Anal. Chem.* **2021**, *93*, 3258−3265.

(20) Das, S. K.; Bhanja, P.; Kundu, S. K.; Mondal, S.; Bhaumik, A. *ACS Appl. Mater. Interfaces* **2018**, *10*, 23813−23824.

(21) Hisaki, I.; Suzuki, Y.; Gomez, E.; Ji, Q.; Tohnai, N.; Nakamura, T.; Douhal, A. *J. Am. Chem. Soc.* **2019**, *141*, 2111−2121.

(22) Yu, T.; Ou, D.; Yang, Z.; Huang, Q.; Mao, Z.; Chen, J.; Zhang, Y.; Liu, S.; Xu, J.; Bryce, M. R.; Chi, Z. *Chem. Sci.* **2017**, *8*, 1163−1168.

(23) Shen, Y.; Shan, B.; Cai, H.; Qin, Y.; Agarwal, A.; Trivedi, D. B.; Chen, B.; Liu, L.; Zhuang, H.; Mu, B.; Tongay, S. *Adv. Mater.* **2018**, *30*, No. e1802497.

(24) Feng, J.-f.; Liu, T.-F.; Cao, R. *Angew. Chem., Int. Ed.* **2020**, *59*, 22392−22396.

(25) Han, B.; Wang, H.; Wang, C.; Wu, H.; Zhou, W.; Chen, B.; Jiang, J. *J. Am. Chem. Soc.* **2019**, *141*, 8737−8740.

(26) Yang, W.; Wang, J.; Wang, H.; Bao, Z.; Zhao, J. C. G.; Chen, B. *Cryst. Growth Des.* **2017**, *17*, 6132−6137.

(27) Yang, W.; Li, B.; Wang, H.; Alduhaish, O.; Alfooty, K.; Zayed, M. A.; Li, P.; Arman, H. D.; Chen, B. *Cryst. Growth Des.* **2015**, *15*, 2000−2004.

(28) Bhuiyan, M. S.; Ellett, F.; Murray, G. L.; Kostoulias, X.; Cerqueira, G. M.; Schulze, K. E.; Mahamad Maifiah, M. H.; Li, J.; Creek, D. J.; Lieschke, G. J.; Peleg, A. Y. *P Natl. Acad. Sci* **2016**, *113*, 9599.

(29) Sanford, A. A.; Rangel, A. E.; Feagin, T. A.; Lowery, R. G.; Argueta Gonzalez, H. S.; Heemstra, J. M. *Chem. Sci.* **2021**, *12*, 11692−11702.

(30) Das, S. K.; Chowdhury, A.; Chakraborty, D.; Kayal, U.; Bhaumik, A. *Mol. Catal.* **2020**, *497*, 111198.

(31) Wang, Y. W.; Nan, L. J.; Jiang, Y. R.; Fan, M. F.; Chen, J.; Yuan, P. X.; Wang, A. J.; Feng, J. J. *Analyst* **2020**, *145*, 2758−2766.

(32) Zhu, J. H.; Feng, Y. G.; Wang, A. J.; Mei, L. P.; Luo, X.; Feng, J. J. *Biosens. Bioelectron.* **2021**, *181*, 113158.

(33) Fan, M. F.; Wang, H. M.; Nan, L. J.; Wang, A. J.; Luo, X.; Yuan, P. X.; Feng, J. J. *Anal. Chim. Acta* **2020**, *1097*, 78−84.

(34) Sun, R. M.; Zhang, L.; Feng, J. J.; Fang, K. M.; Wang, A. J. *J. Colloid Interface Sci.* **2021**, *608*, 2100−2110.

(35) Dai, H.; Chen, D.; Cao, P.; Li, Y.; Wang, N.; Sun, S.; Chen, T.; Ma, H.; Lin, M. *Sens. Actuator B Chem.* **2018**, *276*, 65−71.

(36) Li, Y.; Wu, S.; Huang, L.; Wang, J.; Xu, H.; Li, H. *Mater. Lett.* **2014**, *137*, 281−284.

(37) Rong, M.; Yang, L.; Wang, L.; Xing, H.; Yu, J.; Qu, H.; Liu, H. *Ind. Eng. Chem. Res.* **2019**, *58*, 17369−17379.

(38) Ruiz Osés, M.; González Lakunza, N.; Silanes, I.; Gourdon, A.; Arnau, A.; Ortega, J. E. *J. Phys. Chem. B* **2006**, *110*, 25573−25577.

(39) Xiong, Z.; Zhang, X.; Liu, L.; Zhu, Q.; Wang, Z.; Feng, H.; Qian, Z. *Chem. Sci.* **2021**, *12*, 10710−10723.

(40) Ma, S.; Zhang, J.; Qian, J.; Chen, J.; Xu, B.; Tian, W. *Adv. Opt. Mater.* **2015**, *3*, 763−768.
(41) Wang, X. T.; Jiang, Y. R.; Huang, L. Y.; Gu, Y. X.; Huang, X. Q.; Wang, A. J.; Yuan, P. X.; Feng, J. J. *Analyst* **2021**, *146*, 5995.
(42) Fang, Y.; Wang, H. M.; Gu, Y. X.; Yu, L.; Wang, A. J.; Yuan, P. X.; Feng, J. J. *Anal. Chem.* **2020**, *92*, 3206−3212.
(43) Benson, C. R.; Hui, A. K.; Parimal, K.; Cook, B. J.; Chen, C. H.; Lord, R. L.; Flood, A. H.; Caulton, K. G. *Dalton Trans.* **2014**, *43*, 6513−6524.
(44) Cheng, H. C.; Chiu, K. Y.; Tu, Y. J.; Yang, T. F.; Su, Y. O. *Org. Lett.* **2013**, *15*, 3868−3871.
(45) Beaudoin, D.; Wuest, J. D. *Chem. Rev.* **2016**, *116*, 258−286.
(46) Richter, M. M.; Bard, A. J.; Kim, W.; Schmehl, R. H. *Anal. Chem.* **1998**, *70*, 310−318.
(47) Huang, L. Y.; Hu, X.; Shan, H. Y.; Yu, L.; Gu, Y. X.; Wang, A. J.; Shan, D.; Yuan, P. X.; Feng, J. J. *Sens. Actuator B Chem.* **2021**, *344*, 130300.
(48) Wang, H. M.; Fang, Y.; Yuan, P. X.; Wang, A. J.; Luo, X.; Feng, J. J. *Electrochim. Acta* **2019**, *310*, 195−202.
(49) Wang, C. C.; Wang, H. M.; Fan, M. F.; Fei, L.; Luo, X.; Feng, J. J.; Yuan, P. X.; Wang, A. J. *Sens. Actuator B Chem.* **2019**, *290*, 203−209.
(50) Yang, J.; Xia, Q.; Guo, L.; Luo, F.; Dong, Y.; Qiu, B.; Lin, Z. *Chem. Commun.* **2020**, *56*, 6692−6695.
(51) Danis, A. S.; Potts, K. P.; Perry, S. C.; Mauzeroll, J. *Anal. Chem.* **2018**, *90*, 7377−7382.
(52) Kwon, M.; Park, Y.; Lee, J. H. *RSC Adv.* **2015**, *5*, 94629−94634.
(53) Liang, Z.; Zhang, Q.; Nie, Y.; Zhang, X.; Ma, Q. *Anal. Chem.* **2020**, *92*, 9223−9229.
(54) Kitte, S. A.; Gao, W.; Zholudov, Y. T.; Qi, L.; Nsabimana, A.; Liu, Z.; Xu, G. *Anal. Chem.* **2017**, *89*, 9864−9869.
(55) Chen, Z.; Lai, G.; Liu, S.; Yu, A. *Sens. Actuator B Chem.* **2018**, *273*, 1762−1767.

Recommended by ACS

Dual-Ligand Lanthanide Metal–Organic Framework for Sensitive Ratiometric Fluorescence Detection of Hypochlorous Acid

Yi-Qing Sun, Xue-Bo Yin, *et al.*
FEBRUARY 11, 2021
ANALYTICAL CHEMISTRY
READ

Mixed-Ligand-Regulated Self-Enhanced Luminous Eu-MOF as an ECL Signal Probe for an Oriented Antibody-Decorated Biosensing Platform

Hui Dong, Qin Wei, *et al.*
SEPTEMBER 08, 2022
ANALYTICAL CHEMISTRY
READ

Zinc-Based Metal–Organic Framework with MLCT Properties as an Efficient Electrochemiluminescence Probe for Trace Detection of Trenbolone

Xianzhen Song, Qin Wei, *et al.*
SEPTEMBER 29, 2022
ANALYTICAL CHEMISTRY
READ

Dual-Function Lanthanide–Organic Frameworks Based on a Zwitterionic Ligand as a Ratiometric Thermometer and a Selective Sensor for Nitroaromatic Explosives

Ting Zhou, Huadong Guo, *et al.*
JULY 29, 2021
INDUSTRIAL & ENGINEERING CHEMISTRY RESEARCH
READ

Get More Suggestions >

https://doi.org/10.1021/acs.analchem.1c04608
Anal. Chem. 2021, 93, 17110−17118